

Energies of steps, kinks, and defects on Ag{100} and Ag{111} using the embedded atom method, and some consequences

R.C. Nelson¹, T.L. Einstein^{*}, S.V. Khare

Department of Physics, University of Maryland, College Park, MD 20742-4111, USA

and

P.J. Rous

Department of Physics, University of Maryland, Baltimore County, Baltimore, MD 21228, USA

Received 17 March 1993; accepted for publication 16 June 1993

Using the embedded atom method (EAM) we compute the energies of principal steps, kinks, and single-layer clusters of adatoms (islands) and of vacancies for Ag{100} and Ag{111}. The energies are semiquantitatively consistent with experiments. Comparisons are frequently made with estimates based on nearest-neighbor bond counting. On Ag{111} and Pt{111} the ratio of the energies of the two close-packed steps is closer to unity than measured in experiments on Pt. The energies of clusters are essentially proportional to their perimeter, providing an easy way to estimate the binding energy of clusters to step edges. Adatom-vacancy symmetry is a good approximation except for single-site defects. Our calculations of barriers for single-atom diffusion near steps, compared to across terraces, are consistent with the fractal-like fingered growth of islands experimentally observed on {111} but not seen on {100}. Computed spring constants of surface atoms suggest small changes in perpendicular vibration frequencies near step edges.

1. Introduction

Given the many recent experimental investigations of vicinal surfaces, it is of particular timeliness and interest to compute the microscopic energies which characterize such systems: the energies of steps, kinks on the steps, clusters of adatoms or vacancies on terraces, interactions between kinks or between steps, etc. Such energies are useful to check one's understanding, to guide the choice of material to achieve certain properties, and to parametrize general models. In the latter context, statistical mechanics models of vicinal surfaces invariably make simplifying as-

sumptions about the energetics; many of these assumptions have never been systematically tested.

Because of the low symmetry of these problems, it is very difficult, if not impossible, at this time to compute these energies from first principles. For late transition and noble metals, the semiempirical embedded atom method (EAM) [1] has provided an approximate way to calculate total energies from a local standpoint. The scheme has successfully accounted for a number of surface properties including surface phonons [2–4], surface diffusion [5–8], shapes of adsorbed clusters [9], and reconstruction [10,11]. While its assumptions become less reliable when the coordination of atoms is much lower than in the bulk, it has generally proved to be a tenable approach, particularly for late transition or noble metals, and accordingly has won great popularity.

^{*} To whom correspondence should be addressed.

¹ Present address: Department of Physics, United States Military Academy, West Point, NY 10996, USA.

Specifically, in EAM one computes the total energy of a system of metal atoms using the Ansatz

$$E_{\text{coh}} = \sum_i F_i \left[\sum_{j \neq i} \rho_j^a(R_{ij}) \right] + \frac{1}{2} \sum_{i,j (j \neq i)} \phi_{ij}(R_{ij}). \quad (1.1)$$

Here ρ_j^a is the spherically averaged atomic density of the j th atom (obtained from a parametrically weighted sum of s-type and p-type Hartree-Fock wave functions), F_i is the embedding function of atom i in the linear superposition of the tails of its neighbors, and ϕ is the Coulomb interaction between electronic cores. Except where stated otherwise, we took our F_i 's from Foiles, Baskes, and Daw's "Universal 3" set (FBD-U3) [12]. Our computations used the energy minimization portion of the "DYNAMO" code (version 7.6) to compute energies at zero temperature. A major weakness in using standard EAM for this sort of problem is the neglect of the large gradient in the charge density near the surface. (The procedure to include gradient corrections has been derived formally [14] and implemented computationally for Au{110} [11].) All in all, our results should be regarded as semi-quantitative: better than "ballpark estimates" but not reliable within say 10% of actual energies; inclusion of gradient corrections would probably improve the estimates but not affect general trends. However, trends characterized by energy differences between configurations of less than say 5% may well be questionable. (In fact, in our

analysis of the trends in the energetics of patterned growth of vacancy and adatom clusters in section 4, we often ignore such small differences between similar steps and characterize a family of such steps by their average change in energy.)

In the present study we apply EAM to Ag surfaces vicinal to the {100} and {111} planes (with occasional digressions to Pt). After discussing formal definitions (section 2.1) and computational approaches (2.2), we present the energies of steps (2.3 and 2.4) and kinks (2.5), collected for convenience in table 1. We proceed to consider the shapes of Pt islands (2.6) and the possible propensity to step doubling (2.7). In studies of clusters of adatoms or vacancies on such surfaces (section 3), we find that their energies, at least in the EAM framework, depend on the perimeter of the cluster, almost exclusively on its length and marginally on its shape and orientation; a nearest-neighbor bond picture accounts quite well for most of the properties of these structures, as well as the step and kink energies mentioned above. Our results are consistent with the independent findings of Wolf [15], who parameterized the contributions of nearest and next-nearest neighbor energies to the surface energies of 85 different free surfaces of Au. With a bond energy $v \approx 10^2$ meV, the bond-counting idea provides a good first estimate. On the other hand, the bond energy that best reproduces the precise (EAM) energies depends somewhat on the face and/or the average coordination in the problem. (Moreover, it is widely recognized [16,17] that the bulk cohesive energy is severely underes-

Table 1

The step energies and kink energies calculated for the five common steps on Ag{100} and Ag{111} surfaces, using EAM "Universal-3" (FBD-U3) functions [12]

| Terrace | Microfacet | Name | Step axis | Step energy, β | Kink energy, ϵ (meV) |
|---------------------|------------|-----------------|---------------------------|-------------------------------------|-------------------------------|
| {100} ^{a)} | {111} | Straight | [01 $\bar{1}$] | 102–105 [v] meV/ a_1 | 102 [v] |
| {100} | | Jagged | [001] | 201 [$2v$] meV/ $(a_1\sqrt{2})$ | |
| {111} ^{b)} | {100} | A, straight | [011] | 188 (222) [$2v$] meV/ a_1 | 102 [v] |
| {111} | {111} | B, straight | [$\bar{1}$ 10] | 190 (226) [$2v$] meV/ a_1 | 99 [v] |
| {111} | | Simplest jagged | [$\bar{1}$ 2 $\bar{1}$] | 191 [$2v$] meV/ $(a_1\sqrt{3}/2)$ | |

Parentetical values were computed using Voter-Chen functions [13,22]. Values in brackets are the energies in a nearest-neighbor bond picture, with v the nearest-neighbor bond energy. The nearest-neighbor spacing, a_1 , is $4.09 \text{ \AA} / \sqrt{2} \approx 2.89 \text{ \AA}$.

^{a)} {100} $f_0 \equiv f_{100} = 366$ (459) [$4v$] meV/ a_1^2 (ref. [7]).

^{b)} {111} $f_0 \equiv f_{111} = 279$ (419) [$3v$] meV/ $(a_1^2\sqrt{3}/2)$ (ref. [7]).

timated by the bond energy appropriate to surface problems.) In several of the tables of EAM results, we also include the estimates based on bond-counting. As an intermediate between the simplest bond-counting picture and the full calculation for clusters, we developed sets of rules which can be applied to predict the energy of a randomly selected adatom or vacancy configurations. We discuss implications for describing the statistical mechanics of these metals with lattice-gas models (section 3.5) and for estimating the binding of islands to steps (3.6). Again, a particularly intriguing problem, for which bond-counting is inadequate, is the ratio of the energies of the two kinds of straight steps, called A and B, on a {111} surface (2.6). On Pt B is preferred over A decidedly in experiment and marginally in EAM; for Ag, EAM favors A marginally.

The final portion of the study concerns potential barriers to diffusion of adatoms and vacancies on Ag{100} and Ag{111} (section 4) and calculations of the ratios between spring constants of

adatoms vibrating perpendicularly to terraces near and far away from steps (section 5). We compare our potential barrier results to those from Voter's dynamical simulations [13]. We study how diffusion across terraces compares with diffusion near steps. In considering vibrations we used only static models and thus computed only theoretical spring constants for adatom motion normal to the surface; nonetheless, the *ratios* of these constants are useful for comparison with other calculations and possible observations. In the final section (6), we offer some closing remarks about our findings and open issues.

2. Steps and kinks

2.1. Formal background

As we shall see shortly, the precise meaning of step energy is not so unambiguous as it seems for simple surfaces. Thus, we begin with some formal

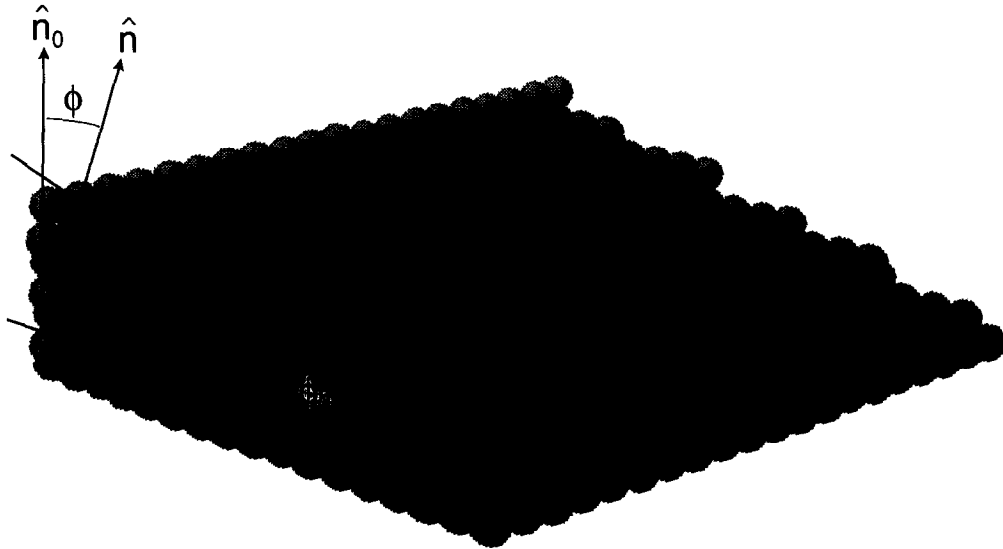


Fig. 1. Portion of a $(3, \bar{2}, 16)$ surface, vicinal to an fcc (001), to illustrate the formal discussion in sections 2a and 2b. The vicinal-surface and terrace normals are $\hat{n} = (3, -2, 16)/\sqrt{269}$ and $\hat{n}_0 = (0, 0, 1)$, respectively. The polar angle ϕ (with respect to the (001) direction) is $\cos^{-1}(16/\sqrt{269})$, while azimuthal angle θ , indicating how much \hat{n} is rotated around \hat{n}_0 away from the vertical border on which ϕ_0 is marked, is clearly $\arctan(1/5)$; $\tan \phi_0 = \tan \phi \cos \theta$. Since h is $a_1/\sqrt{2}$, where a_1 is the nearest-neighbor spacing, the mean distance ℓ (in a terrace plane) between steps is $a_1/(\sqrt{2} \tan \phi) = 8\sqrt{2}/13 a_1 \approx 3.138a_1$. While the average distance from one step to the next along a principal, $\langle 110 \rangle$ direction looks like $3.5a_1$, it is in fact $a_1/(\sqrt{2} \tan \phi_0) = 3.2a_1$. The "projected area" of this surface segment, used to compute the surface free energy f , is the size of an (001) layer:

$$20a_1 \times 17a_1 = 340a_1^2; \text{ the width } W \text{ is } 20a_1.$$

definitions, which we illustrate in fig. 1. For vicinal surfaces, tilted by an angle ϕ from a low-index face, we consider the surface free energy per unit *projected* area $f(\phi, T)$ (the projection being onto the low-index plane of the terraces); in particular, $f(\phi, T)$ can be expanded with respect to the (average) density of steps [18,19]

$$f(\phi, T) = f_0(T) + \beta(T) \frac{|\tan \phi|}{h} + g(T) |\tan \phi|^3. \quad (2.1)$$

In this equation the first term is the surface free energy per unit area of the terrace orientation. The average density of steps (i.e. the inverse of their mean separation) is $|\tan \phi|/h$, where h is the step height. In the second term $\beta(T)$ is the *free energy per unit length* of step formation. The third term is a step interaction term, about which we shall say little in this paper. We emphasize that in order for β to be well defined, one must specify clearly what constitutes the step and so, at least implicitly, specify the orientation of the terraces between the steps, i.e. the orientation onto which areas are to be projected. To highlight this assertion, we consider the (311) face of an fcc crystal. This surface can be viewed as vicinal to either (111) or (100) [20], with the terrace for one orientation being the riser for the other, and vice versa. We find that what we call β is almost twice as large when the surface is viewed as vicinal with respect to (111): 76 meV/Å with respect to (111) versus 40 meV/Å with respect to (100).

Vicinal surfaces whose steps have periodic kinks can be produced by certain combinations of polar and azimuthal rotations, as shown in fig. 1. Such individual kinks are the lowest-order excitation of the stepped surface and lead via the wandering (diffusivity) of the step to the decrease in its free energy at finite temperature. (See section 2.6 for an application.) At zero temperature, the energy of the surface becomes

$$f(\phi_0, \theta) = f_0 + \frac{\tan \phi_0}{h} \left(\beta(0) + \frac{\epsilon}{b} \tan \theta \right). \quad (2.2)$$

Here θ is the azimuthal angle between a periodically kinked step and a principal axis, ϕ_0 the tilt angle about this direction, and b is the spacing between rows of the surface perpendicular to the step edge, so that the mean $(1-d)$ density of kinks along a step edge is $b^{-1} \tan \theta$; ϵ is the additional energy contributed by an individual kink. It is, of course, more usual to express f in terms of the polar angle ϕ between the surface normal and the terrace normal; then

$$f(\phi, \theta) = f_0 + \frac{\tan \phi}{h} \left[\beta(0) \cos \theta + \frac{\epsilon}{b} \sin \theta \right], \quad (2.2')$$

the bracketed term being reminiscent of Kossel crystals (i.e., just nearest-neighbor interactions) [21]. In the general case the “side” of the kink, i.e. the excursion away from the step direction, is not perpendicular to this direction.

2.2. Computational approach

In an actual computation, we first consider a thick flat rectangular slab consisting of $\mathcal{N}_\square = NL$ atoms, with two opposing faces oriented in a high-symmetry direction (viz. {100} or {111}). Each face, and each of the $L-2$ interior layers, contains N atoms. Periodic boundary conditions are applied in the other two directions, and some of the central layers may be frozen in bulk positions relative to each other. From the total energy of this flat slab \mathcal{E}_\square , we calculate the surface energy per area, f_0 , using

$$\mathcal{E}_\square - \mathcal{N}_\square E_{\text{bulk}} = 2A_\square f_0, \quad (2.3)$$

where E_{bulk} is the bulk energy, specifically $-2.85\mathcal{N}$ eV for Ag, and A_\square is the area of each side of the flat slab, i.e. N times the area of a unit cell on the surface. (While the driving package lists automatically the embedding energy of each atom, it is the total energy that is the most important physically as well as the least dependent on user choices. Nonetheless, these energies of individual sites can sometimes prove helpful in checking physical ideas.)

To compute the step energy, we next consider either slabs having high-Miller-index planes top

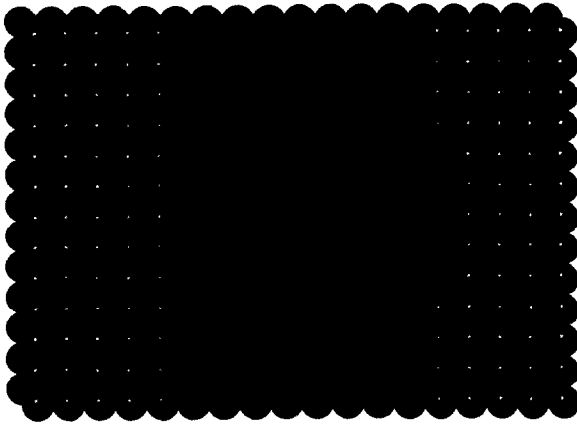


Fig. 2. Example of a groove on a {100} surface, used to compute the energy of straight steps. The right side has an added indentation, used to compute the associated kink energy. The top layer is a lighter shade to improve clarity; all atoms are the same. Note that the projected area of this surface is identical to the corresponding flat (ungrooved) surface; likewise, the projected length of both steps is the same.

and bottom, with periodic arrays of steps relative to the closer-packed terrace planes, or the earlier slab with wide, single-layer height grooves of atoms removed to create step and “antistep” pairs on one side, as illustrated in fig. 2. (Typically the opposing, ungrooved surface and a few layers in from it are “frozen” in their bulk configuration in this case. The distance over which the atoms are frozen need not exceed the cut-off distance for interatomic interactions.)

For most theoretical calculations of statistical properties of vicinal surfaces, the {100} simple cubic lattice is chosen. Also, this lattice surface is almost always used in illustrations of stepped, kinked, or rough surfaces; accordingly, its special simple properties color much of our thinking. For this simple case, it is relatively easy to find the step energy, since the riser does not affect the projected area. Then the step energy per unit length β is just the excess energy of the stepped slab \mathcal{E}_{st} compared to \mathcal{E}_{fl} of the corresponding “flat” one, divided by the *total* number of steps \mathcal{N}_s and by the length of one of these steps, typically the width W of the slab. To estimate β , one could take the surface free energy per area of a plane with the orientation of the riser and

multiply by the distance d across the riser, where here d is just h , the step height. Corrections would come from the upper and lower right-angle “creases” and relaxations near the step.

In general the step riser planes connecting atoms at the top and bottom “creases” of a step, i.e. the microfacets associated with the step, will not be perpendicular to the terraces. Neglecting contributions from the creases and relaxation, the step energy can again be readily estimated. Again one starts with the free energy per area of the microfacet of the riser, multiplied by d . Reminiscent of an awning shading a smaller area beneath it, the step removes some of the lower terrace plane, so one must *subtract* the free energy associate with this lost area along the terrace, i.e. the free energy per area of the terrace plane times the projection of d onto the terrace plane, i.e. $\sqrt{d^2 - h^2}$. For example, consider a step in a square-lattice principal direction on a {100} fcc crystal. (Cf. the straight parts of the steps in fig. 1.) The riser is a {111} microfacet. Denoting the nearest-neighbor spacing a_1 , we see in this case that $d = a_1(\sqrt{3}/2)$ and $h = a_1(\sqrt{2}/2)$, so that the projection of d is $\frac{1}{2}a_1$. Then

$$\beta_{100\text{-str}} \approx \left(\frac{\sqrt{3}}{2} f_{111} - \frac{1}{2} f_{100} \right) a_1, \quad (2.4)$$

where f_{100} and f_{111} are the f_0 's for {100} and {111} planes, respectively. In the example of the (311) surface cited above, both the contribution from the microfacet and the subtracted contribution from its projected area times the terrace energy differ depending on which plane is chosen as the terrace, i.e. to which orientation it is vicinal.

Another common, natural way of discussing the energy of a step is to focus on the *net* change in number of nearest-neighbor bonds due to its presence. This “changed-coordination” energy is independent of the choice of terrace orientation. In this bond-atom perspective the terrace dependence comes from an additional term due to the need to treat more atoms as being surface atoms, so that there is an “excess surface area”. This approach is applied below to account for the principal step energies. (For estimating energies

and gaining insight, the preceding “awning” method is more straightforward and usually more accurate.)

To compare with a flat slab, it is simplest to use a stepped surface, vicinal or grooved, with the same *projected* area; then no adjustment is needed to normalize the area of \mathcal{E}_{st} relative to \mathcal{E}_{fl} , so that

$$\mathcal{E}_{\text{st}} - \mathcal{E}_{\text{fl}} - (\mathcal{N}_{\text{st}} - \mathcal{N}_{\text{fl}})E_{\text{bulk}} = \mathfrak{N}_s \beta W \quad (2.5)$$

(for $A_{\text{st}} \hat{n} \cdot \hat{n}_0 = A_{\text{fl}}$),

where \hat{n} and \hat{n}_0 are the orientations of the vicinal surface and the terrace, respectively. (Cf. fig. 1.) The area of a face of the vicinal surface and the number of atoms in the associated slab are denoted A_{st} and \mathcal{N}_{st} , respectively, with $A_{\text{st}} \hat{n} \cdot \hat{n}_0$ the projected area. (For a grooved surface, the projected area is the same as the flat surface by construction.) The right-hand side of eq. (2.5), then, is the “excess energy” due to steps: the product of the total number, their energy per length, and the slab width. Notice that E_{bulk} serves as a sort of chemical potential for atoms. In the general case for unknicked steps, we first find f_0 from eq. (2.3) and solve for β in

$$\mathcal{E}_{\text{st}} - \mathcal{N}_{\text{st}} E_{\text{bulk}} - 2f_0 A_{\text{st}} \hat{n} \cdot \hat{n}_0 = \mathfrak{N}_s \beta W. \quad (2.6)$$

In computing the kink energy ϵ , we encounter analogous subtleties to those discussed above for the step energy. Again we must assure that, when subtracting the energy of a stepped, kinked slab from one with straight steps, any differences in (projected) length along the step edge direction are multiplied by β and included in the difference: the kink energy is the correction to the energy per projected length of the step. Again, these issues are minimized by working with a grooved surface, now with an indentation as in fig. 2 or a similar protrusion toward the center of the groove.

For vicinal surfaces, the case of primary interest here is simple, unit (perpendicular excursion by b) kinks spaced regularly along an otherwise straight step of nearest-neighbor atoms. If the straight segments are ma_1 long (between the end of a simple kink and the start of the next), then because of the periodic boundary conditions the

excess energy of the step will be an integer (viz. the number of segments) multiple of $(m + \gamma)a_1\beta + \epsilon$, where γ is 0 for {100} and $\frac{1}{2}$ for {111}. Then the generalization of eq. (2.6) amounts to computing the left-hand side of this equation and dividing by the number of kinks on both sides; the result is $(m + \gamma)a_1\beta + \epsilon$, where β is taken from a calculation with unknicked steps. In this procedure the kinks should be sufficiently separated that their interactions do not contribute but close enough so that uncertainties in β from straight steps do not obscure the value of ϵ . Finally, it is crucial that the slab has periodic boundary conditions in the two directions of the vicinal surface. For high-index orientations, this requirement necessitates slabs with large areas A_{st} . (E.g. the illustrative portion in fig. 1 fails this test: while casual inspection might suggest there are 5 steps, with 4 kinks per step, there actually are 21 kinks on this portion. The area of the minimum acceptable slab is nearly three times as large, with a 4×15 array of kink apexes. Also, its bottom side is parallel to the top, so stepped and kinked as well.)

2.3. Steps on Ag{100}

In the simplest approximation (Kossel crystal), the loss of 4 nearest neighbors relative to bulk for each atom on a {100} surface (and so 4 bonds, each with energy v) leads to the estimate of the surface energy per area f_{100} as $4v/a_1^2$. In our computation for Ag{100} we find that the $f_{100} = 366.5 \text{ meV}/a_1^2 = 366.5 \text{ meV}/(4.09 \text{ \AA}/\sqrt{2})^2 = 43.8 \text{ meV}/\text{\AA}^2 = 702 \text{ erg}/\text{cm}^2 = 0.702 \text{ J}/\text{m}^2$. On this relaxed surface, the first layer spacing has decreased 2% from the bulk value. For a truncated bulk lattice, this surface energy would be only 0.7% larger: relaxation reduces f_{100} by less than 1%! Our value of f_{100} is identical to that (viz. 702 erg/cm²) reported by Liu et al. [7] using AFW (Adams–Foiles–Wolfer [5]) EAM functions quite similar to the FBD-U3 potentials we used (with which FBD [12] had computed 705 erg/cm²). With VC (Voter–Chen [13,22]) functions, they [7] found f_{100} to be 25% larger. The main difference between the Sandia functions (AFW and FBD-

U3) and the VC functions is that the latter include experimental data for diatomic molecules in the fitting procedure [7], there is no reason to believe that they are better – or worse – for the present problem, and the disparity gives some feeling for the absolute errors in this sort of calculation. We do emphasize that both kinds of functions give the same semiquantitative trends and physics. Moreover, all the EAM values for surface energies are substantially lower than experimental numbers; this well-known shortcoming can be ameliorated with gradient corrections [11]. For purposes of comparison, note that Todd and Lynden-Bell [23], using the simpler Sutton–Chen model potentials [24], computed $f_{100} = 62 \text{ meV}/\text{\AA}^2$.

In this study we consider two types of steps on Ag{100}. The straight steps proceed along – and can be formed by rotations of the (100) surface around – $\langle 0\bar{1}1 \rangle$, the principal axes of the square surface net. The Miller indices for such surfaces are of the form $(2n + 1, 1, \pm 1)$, where crests or bottoms of neighboring steps are $\ell = (n + 1/2)a_1$ apart along the terrace direction [27,28], i.e. $a_1\sqrt{[(n + 1/2)^2 + 1/2]}$ apart. The second is the lowest-order jagged step on (100) whose axes of rotation are oriented at angles of 45° to the principal axes, with Miller indices $(n + 1, 1, 0)$.

To evaluate the step energy, it is easiest to use a {100} slab from which a broad single-layer groove of atoms was removed, creating a step and an antistep, which in this case is identical to the step. (Cf. fig. 2 without the “indentation”.) Here we found β to be $102.2 \text{ meV}/a_1$, or $35.4 \text{ meV}/\text{\AA}$. From a calculation on a (711) slab, we deduce a step formation energy that is 2% greater: $\beta = 105 \text{ meV}/\text{atomic spacing}$, or $36 \text{ meV}/\text{\AA}$. (With VC functions, we found $\beta = 135 \text{ meV}/a_1$.) This configuration is an example of the non-perpendicular risers discussed above. If we use the awning approximation of eq. (2.4), referring to the next subsection for f_{111} , we would estimate β to be v/a_1 for the Kossel crystal and $96 \text{ meV}/a_1$ with our computed f_0 's.

From the bond–atom perspective, there is a net gain in surface coordination of the atoms at the step of +1/atom (compared to the coordina-

tion of surface atoms, viz. 8); –1 for the atom at the top of the step and +2 for the atom at the bottom. If this were the only consideration, βa_1 would be $-v$! If we associate a square unit cell with each atom at the top and the bottom bend of the step, the squares from top and bottom would overlap a distance b minus the projection of d (see eq. (2.4)), i.e. $\frac{1}{2}b = \frac{1}{2}a_1$. Next, we must choose a calculated quantity from which to evaluate v . Using the surface energy of the microfacet (so $v = 93 \text{ meV}$), we get

$$\beta_{100\text{-str}} \approx \left(-\frac{1}{2\sqrt{3}}f_{111} + \frac{1}{2}f_{100} \right) a_1, \quad (2.7)$$

with a value of $90 \text{ meV}/a_1$. Had we chosen to evaluate v using the terrace free energy (so $v = 91.6 \text{ meV}$), we would have found $\beta_{100\text{-str}} \approx f_{100}a_1/4 = 92 \text{ meV}/a_1$. Either way, the awning viewpoint of eq. (2.4) gives a better estimate. The fact that the changed-coordination reduces β from $183 \text{ meV}/a_1$ has the interpretation that the riser's {111} microfacet has lower surface energy than the terrace.

From a (710) slab we found that the energy of the jagged step is $\beta = +201 \text{ meV}/(\text{apex atom})$, or $50 \text{ meV}/\text{\AA}$. This energy per length is essentially $\sqrt{2}$ larger than for straight steps, consistent with the excess energy coming from links along the edge, with insignificant contributions from corners. There is a slight decrease in energy from strict counting of links: a 6×6 defect “island” has excess energy 2.4463 eV , while if the defect has a diagonal edge (21 missing atoms but the same perimeter), the excess energy is 2.4443 eV . Presumably this negligible difference is due to minor relaxation effects. We will later see that ϵ is also $+102 \text{ meV}$ for {100}, to within small corrections which can be taken as the result of relaxations at the kink site.

2.4. Steps on Ag{111}

The close-packed face of Ag is the most stable facet. With 3 lost bonds per surface atom, a Kossel crystal has $f_{111} = 3v/[(\sqrt{3}/2)a_1^2]$. In our EAM calculation $f_{111} = 279 \text{ meV}/[(\sqrt{3}/2)a_1^2] = 39 \text{ meV}/\text{\AA}^2 = 617 \text{ erg}/\text{cm}^2$. (This result is again

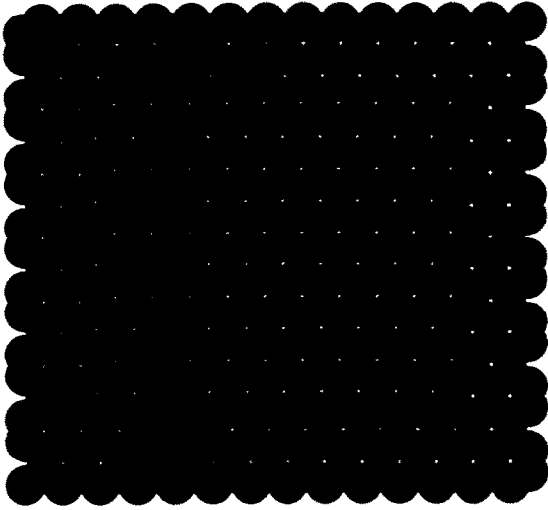


Fig. 3. View of an island (as in fig. 2, shown in a lighter shade strictly for clarity) on a {111} surface. At the top and the bottom are the straight, close-packed A ($\langle 110 \rangle / \{100\}$) and B ($\langle 110 \rangle / \{111\}$) steps, respectively. At both sides is the jagged step, consisting of alternating A and B links.

consistent with earlier calculations with FBD [12] and AFW [7] functions; with VC functions, f_0 is 30% larger [7]. Also, in the calculation [23] using Sutton–Chen potentials, the energy decreased by 7% from the {100} value, compared with our 11% decrease.)

Since the second layer reduces the 6-fold symmetry of the top layer to 3-fold symmetry, two types of straight steps can appear. Specifically, rotations around one of the three $\langle 01\bar{1} \rangle$ directions produce steps of the type pictured at the upper island edge in fig. 3: atoms along the bottom of the step riser are located in positions directly opposite the atoms along the top of the step edge, with a (100) microfacet; accordingly, they have been labeled $\langle 110 \rangle / \{100\}$ [25] or simply A [26]. The Miller indices of such surfaces have the form $(n+2, n, n)$ [27,28]. The distance ℓ in the terrace plane between adjacent steps is $(n + \frac{2}{3})a_1(\sqrt{3}/2)$. (Note, however, that for n even, the surface is conventionally labelled $(n/2 + 1, n/2, n/2)$.) For A steps, $d = a_1$; since $h =$

$(\sqrt{6}/3)a_1$, we find the “awning” estimate (cf. eq. (2.4)) to be

$$\beta_A \approx \left(f_{100} - \frac{\sqrt{3}}{3} f_{111} \right) a_1. \quad (2.8)$$

For a Kossel crystal β_A is then $2v/a_1$, while with our evaluations of the f_0 's we could estimate β_A as $180 \text{ meV}/a_1$. Our calculation shows the energy of this type of step is $+188 \text{ meV}/a_1$, or $65 \text{ meV}/\text{\AA}$. (With VC functions, we find this step energy to be $222 \text{ meV}/a_1$. With Sutton–Chen, it is $174 \text{ meV}/a_1$ [29].)

From fig. 3, one can see that the coordination numbers of the atoms along the top and bottom edges are 7 and 10, respectively. Since the coordination number of a terrace atom is 9, the step produces a net *loss* of one nearest-neighbor bond per atomic spacing, i.e. a contribution to β of v/a_1 . Since the overlap distance is $b/3$, the “excess projected area” per a_1 is $(1/3)(\sqrt{3}a_1/2)$. Repeating the choices made in reaching eq. (2.7), we find

$$\beta_A \approx \left(\frac{1}{4} f_{100} + \frac{\sqrt{3}}{6} f_{111} \right) a_1, \quad (2.9)$$

which leads to $\beta_A = 185 \text{ meV}/a_1$, closer to the EAM value than the evaluation of eq. (2.8). Had we used the terrace energy to get v , we would have obtained $\beta_A \approx f_{111} a_1 / \sqrt{3} \rightarrow 186 \text{ meV}/a_1$.

Finally, note that in the introductory example of a {311} surface, the factor of nearly 2 is just the ratio of β_A to β for straight steps on {100}. Both {311} step energies are greater than their counterparts above because repulsions between the steps become sizable at small ℓ (and n is 1 for either terrace orientation). With care one can sort out these effects to separate the effective β into its large- ℓ value, such as discussed in sections 2.3 and 2.4 and listed in table 1, and the interaction part associated with the last term in eq. (2.1).

The second type of step is produced by rotation of Ag(111) around $\langle 0\bar{1}1 \rangle$, as occurs at the lower island edge in fig. 3. The Miller indices of such vicinal surfaces are $(n+1, n+1, n-1)$, $\ell = (n+1/3)a_1(\sqrt{3}/2)$. The atoms along the bottom of the step edge are now interspaced with

the atoms along the top edge. Since the microfacet structure of this close-packed riser is {111}, this step has been called $\langle 110 \rangle / \{111\}$ [25] or simply B [26]. In this case, $d = (\sqrt{3}/2)a_1$, so that in the awning approximation

$$\beta_B \approx (f_{111} - \frac{1}{3}f_{111})a_1 \frac{\sqrt{3}}{2} = f_{111}a_1/\sqrt{3}. \quad (2.10)$$

For a Kossel crystal β_B is then $2v/a_1$, identical to β_A . With our computed f_{111} , eq. (2.10) leads to the estimate 186 meV/ a_1 for β_B . In the full calculation β_B is +190 meV/ a_1 . (With VC functions, β_B is 226 meV/ a_1 .)

Since the coordination numbers of the top and bottom edge atoms are 7 and 11, respectively, there is no net loss of nearest-neighbor bonds and so no contribution from changed coordination. Since the overlap is twice as large as for A steps, so is the excess area contribution $\frac{2}{3}(\sqrt{3}a_1/2)f_{111}$, reproducing eq. (2.10)! Notice also that in the alternative to eq. (2.9), β_A also is $f_{111}a_1/\sqrt{3}$, a reason why we chose to get v from the terrace. To assess the validity of the role of coordination, we examined the embedding energies of individual atoms, supplied automatically by the driving program, DYNAMO. The atoms along the top edges of A and B steps have nearly the same cohesive energies (-2.38 eV), while most of the difference between the energies of the two types of steps comes from the tighter binding of the atoms at the bottom of B steps (-2.75 eV versus -2.68 eV).

For assessing the accuracy of the energies given throughout the paper, the benchmark value of +95.4 meV/nearest-neighbor bond compares as well as could be expected to the value obtained by Poensgen et al. [16] for the kink activation energy on Ag{111} of $E_k \approx +75.5 \pm 2.2$ meV through analysis of scanning tunneling microscopy scans. The basic conclusion is that the energies of the two straight steps on Ag{111} are almost identical, with the A step slightly more favorable.

A jagged step is formed by rotation around an axis which is oriented at 90° to any of the six previously described directions; the Miller indices for such a periodically stepped surface are $(n +$

$3, n + 1, n - 1)$. Identical zig-zag steps are formed for either direction of rotation. It consists of alternating units of A and B steps, each of intrinsic length a_1 and so $a_1 \cos 30^\circ$, or $0.866a_1$, along the *mean* direction of the step edge. The energy per unit should be the average of the two step energies found above, if corners are insignificant (which we shall see shortly is a good approximation for the cases in this paper). From a calculation of a grooved surface, we find β is +193 meV per unit length ($\sqrt{3}a_1/2$). The calculation for the vicinal surface illustrates how eq. (2.6) is actually used. Subtracting the bulk energy from the final EAM energy of a Ag(432) (i.e. (864)) block, then dividing by the projected area ($\text{area} \times \cos \phi$) of both free surfaces, we get $f(\phi, 0) = 47.3 \text{ meV}/\text{\AA}^2$. Subtracting $f_{111} = 38.5 \text{ meV}/\text{\AA}^2$ and multiplying the difference by the terrace width we find $\beta = 79.13 \text{ meV}/\text{\AA} = +191 \text{ meV/unit length}$.

To make estimates, the awning method is not helpful since we do not know f_0 of the riser orientation. In the bond-atom method, note that alternate atoms (those step tips) have a coordination number 6, while the atoms spaced back at the inner corner have coordination number 8. The corresponding atoms along the bottom of the step edge have coordination numbers 10 and 11, respectively. On average there is a net loss of half a nearest-neighbor bond for every atom along the jagged edge. The excess area is also the average, per link, of the A and B steps. Thus,

$$\begin{aligned} \beta &\approx \left(\frac{1}{2}v + \frac{\sqrt{3}}{4}f_{111}a_1^2 \right) / \left(a_1 \frac{\sqrt{3}}{2} \right) \\ &= \left(\frac{\sqrt{3}}{3}f_{111}a_1^2 \right) / \left(a_1 \frac{\sqrt{3}}{2} \right), \end{aligned} \quad (2.11)$$

where we have obtained v from the terrace energy; the value is 186 meV per unit length of $(\sqrt{3}/2)a_1$.

Finally, we computed a Wulff plot for orientations between [100] and [111], as displayed in fig. 4. There are evidently no intermediate cusps, so that only these two orientations are facets. When nearest-neighbor interactions dominate, the 3D polar plot of the surface free energy lies on a sphere passing through the origin [30]. The

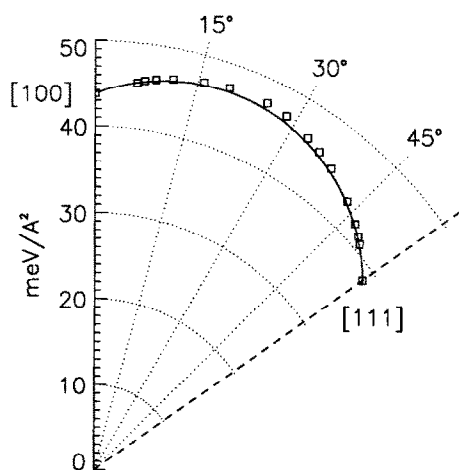


Fig. 4. Segment of the zero-temperature Wulff plot (surface energy computed with EAM versus orientation) along the azimuth connecting the (100) and (111) facets. The solid curve is an arc of the circle passing through the origin and through the two points representing these facets. If only nearest-neighbor interactions determine the surface tensions, the points should lie on this arc [30]. Evidently the EAM energies are well described by this approximation.

curve in fig. 4 has the form of the concomitant circular arc, consistent with Wolf's finding [15] for Au using EAM. He noted that allowing relaxation actually improves the approximation of nearest-neighbor dominance.

2.5. Kinks

In striking contrast with semiconductor surfaces, the kink energies for metals which are well described by near-neighbor models are rather simple to characterize since they are ipso facto overwhelmingly due to the step energy of the extra sides of the kink. For Ag{100}, the side of the kink is perpendicular to the direction of straight steps (consistent with the 4-fold symmetry of the surface). From calculations on grooved surfaces with rectangular notches we find that the energy of the kink is 102.2 eV, corresponding to an extra link of straight step. The corner energy is negligible. (For Si{100} [31], the corner energy was about three times the energy of a side link!)

For the {111} surface, kinks are not perpendicular to steps, so that one must be careful to

compare kinked and unkinked steps with the same *projected* length, i.e. length projected onto the direction of the unkinked step; if there is a difference, one must make adjustments analogous to those for non-perpendicular risers. By putting notches into the sides of single-layer-depth defects, we deduce kink energies of 102 meV for A steps and 99 meV for B steps. To explicate these kink energies, we note that the kink on an A step is a unit of B step, with energy 190 meV. However, the kink eliminates $\frac{1}{2}a_1$ of A step, saving energy 94 meV. The fact that the kink energy is 102 meV rather than 96 meV suggests that corner energies are still small but not completely negligible. By similar arguments, one would predict that the kink on B would cost $188 - \frac{1}{2} \times 190 = 93$ meV, 3 meV smaller than the 96 meV estimated for the A kink, mirroring the difference of 102 and 99 meV in the actual calculation.

To corroborate this assignment of energies, we considered slabs for several periodically kinked vicinal surfaces. For high Miller index surfaces, the need for rectangular cells with periodic boundary conditions led us to very large systems. For example, to study Ag(12, 8, 7), illustrated in fig. 5, we used a slab with 6500 atoms. The area of the top of the large cluster is 6972.66 \AA^2 , so $\hat{n} \cdot \hat{n}_0 = 0.9724$, the projected area is 6780.08 \AA^2 . Half the difference of the total energy and the bulk energy of the same number of atoms gives a surface energy of 310.5445 eV for the top. Subtracting from this f_0 times the projected area gives an excess of 49.4126 eV due to steps and kinks. Since this surface has 52 kinks, spaced $4\frac{1}{2}a_1$ apart along A steps (i.e. $m_1 = 4$, in the notation of ref. [28]), $4\frac{1}{2}a_1\beta_A + \epsilon$ should be 950.2 meV. With $\beta_A = 188 \text{ meV}/a_1$, this suggests $\epsilon = 104$ meV, versus 102 meV derived earlier, excellent agreement for this sort of calculation. This discussion illustrates clearly that this method to compute ϵ tends to be less accurate than using grooved slabs, since here any error in β is propagated into ϵ with an augmentation factor $4\frac{1}{2}a_1$. If a surface is chosen with more closely spaced kinks, there are questions of kink-kink interactions.

We also generated a 2800-atom slab having B steps, with kinks similarly spaced $4\frac{1}{2}a_1$ apart along

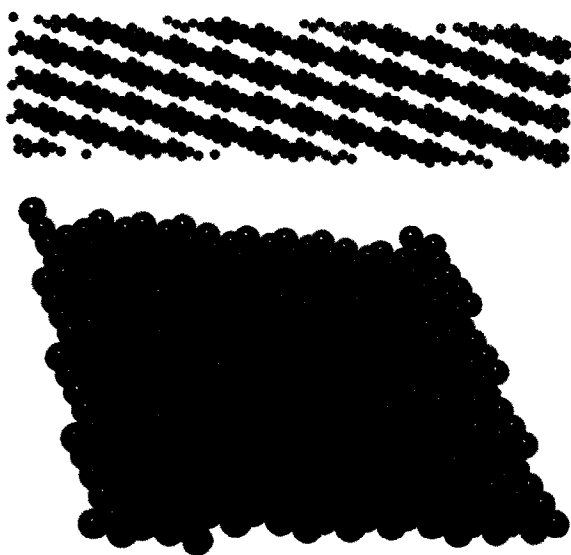


Fig. 5. Two views of a (12, 8, 7) surface, which has periodic kinks as well as steps. More accurate assessments of kink energies can usually be obtained from grooved surfaces such as shown in fig. 2. The lower portion is on a large enough scale so that one can see the structure of the kinks and steps. This portion is not large enough to support screw-periodic boundary conditions; the minimum size needed for a calculation has 4 kinks in one directions and 13 in the other, as depicted in the upper portion with atoms from few enough (12, 8, 7) planes so that one can easily see this overall structure.

the step edge, viz. Ag(21, 19, 11). In a similar computation, we find $4\frac{1}{2}a_1\beta_B + \epsilon = 955.8$ meV. With $\beta_B = 190$ meV/ a_1 , this suggests $\epsilon = 101$ meV, versus 99 meV derived earlier, again close but slightly higher than the value from the grooved surface with kink pairs, where no subtraction of large numbers is needed.

2.6. Shapes of Pt islands

Unfortunately, there is no experimental data for these Ag step energies; however, Michely and Comsa [25] in elegant STM explorations of the equilibrium shapes of islands and monolayer defects on Pt(111) were able to determine that the B step had slightly *lower* free energy than the A step; the ratio β_B/β_A was 0.87 ± 0.02 . To check whether EAM could reproduce this ratio and so reliably predict such shapes for other surfaces, we

evaluated using Pt FBD-U3 EAM functions the A and B step energies to be 344 meV/ a_1 and 341 meV/ a_1 , respectively, for Pt(111). Using Voter–Chen functions, we found these energies to be 359 and 357 meV/ a_1 , respectively. In either case, we see that the B step is now favored, in contrast to Ag, but that the ratio is much closer to unity than in experiment.

The numbers we have computed are simply energies per length, while the experiment probes the *free energy* per length at about 700 K (i.e. ~ 60 meV). To leading order in $\exp(-\epsilon/kT)$, the reduction of β due to the entropy associated with “diffusional” step wandering is [19,32]

$$\beta(T) = \beta(0) - \frac{2kT}{a_{\parallel}} \exp(-\epsilon/kT) \quad (2.12)$$

for geometries such that kinks and “antikinks” have identical energy ϵ [33], a condition satisfied by all the steps covered in table 1. Here $\beta(0)$ is the energy per length of a (straight) kink-free step, such as computed in the preceding subsections, and a_{\parallel} is the distance between sites along the step, viz. a_1 for the straight steps.

According to calculations on a grooved Pt surface using Universal-3 functions, the energies of kinks on A and B steps are 161 and 178 meV, respectively. (Since the kink on A is a B-like link, and vice versa, it is not surprising that the B kink has higher energy. These numbers are averages of outward and inward kinks: for A, these are 158 and 164 meV, respectively; for B they are 176 and 180 meV, respectively. As an added note, these kink energies are found to be 101 and 110 meV, respectively, using a Sutton–Chen potential [34].) We find the A and B step free energies are reduced to 336 and 335 meV/ a_1 , respectively, making the ratio even closer to one, as one would expect from the parenthetical comments.

It is not clear which of the approximations in EAM calculations results in the lack of quantitative accounting for the experimentally observed ratio, nor what precisely determines whether the A or the B step has lower energy. It would be interesting to survey systematically the late transition and noble metals experimentally to see whether at least the favorability of A or B is

accurately reproduced by EAM. We offer an “ap-petizer”: from approximate eqs. (2.8) and (2.10), we see $\beta_B/\beta_A \approx (f_{100}\sqrt{3}/f_{111} - 1)^{-1}$. Using tabulated Pt surface energies computed with FBD [12], AFW [7], and VC [7] functions, we find this ratio to be 1.02, 1.18, and 1.00^- , respectively. (If instead we used eqs. (2.9) and (2.10), then $\beta_B/\beta_A \approx 2(f_{100}\sqrt{3}/2f_{111} + 1)^{-1}$ and the three ratios become 1.004, 1.041, and 1.000.) Thus, the preference for B steps comes from more subtle crease and/or relaxation effects. Since these tables also list values for Cu, Ag, Au, Ni, and Pd, we computed $(f_{100}\sqrt{3}/f_{111} - 1)^{-1}$ for all three sets of functions. Only for Au was this number consistently less than unity (viz. 0.99 in all 3 cases). Except for the anomalous AFW value, Pt was the next smallest. Ni and Cu were consistently between 1.12 and 1.15, Pd somewhat smaller, and Ag midway between Pd and Au. (With the alternative ratio, the same trend emerges, but with ratios much closer to unity.) The trend is somewhat reminiscent of Foiles’s finding [10] that the propensity of {110} fcc metals to reconstruct increased with increasing row number in the periodic table. That behavior was related to competition in EAM between attractive two-body interactions and weak three-body repulsions. Since, again, we have not scrutinized the additional contributions, it is not clear how these trends will carry over to full EAM calculations or, perhaps more importantly, to actual experiments. This whole problem merits more careful investigation.

2.7. Step interactions and doubling

Interactions between steps on a vicinal surface are expected to be repulsive, decaying to leading order as the inverse square power of separation if the interactions are due to elastic or dipolar effects. This idea is implicit in the last term of eq. (2.1); such leading behavior, along with the “entropic repulsion” arising because steps cannot cross, contribute to B [18]. At short range it is not so simple to make analytic predictions. We studied this repulsion briefly within the limits of the model by comparing with the previous results the energy of similar steps but with terrace widths of

only two or three atoms. Since these calculations were performed [35], a more detailed EAM study of <001> steps on vicinal Au{100} and Au{110} found that the step-step repulsion followed the expected behavior from continuum elasticity theory – inverse square of separation – but with a prefactor 1/2 to 1/3 of what would be predicted from the elastic constants [36].

Notwithstanding these entropic and elastic repulsions, energetics sometimes favor the coalescence of neighboring steps which make contact with each other. Depending on longer-range interactions, this effective local attraction can lead either to step-doubling [37] or to coalescence and formation of a low-index microfacet. Accordingly, we examine the energetic consequences of doubling the various types of single-height steps studied above. We are especially interested in {100} and {111} faceting on vicinal surfaces with straight steps. From the Wulff plot of fig. 4, reported earlier, we expect that these will be the only two stable facets along this azimuth, at least in the EAM approximation. We find that doubling is energetically favored when the faceting direction has higher surface density than the terrace direction, and vice versa. When the microfacet has the same symmetry as the terrace, the doubling energy is small in magnitude.

The doubled A step on Ag(111) leads naturally to a [100] microfacet; the additional step energy associated with doubling is $+10.1 \text{ meV}/a_1$. This number is about 5% of the step energy of the corresponding single-height straight step. Since this energy is positive, doubling of A steps is a barrier to formation of {100} microfacets on {111} surfaces. The B step on Ag{111} tends – weakly –

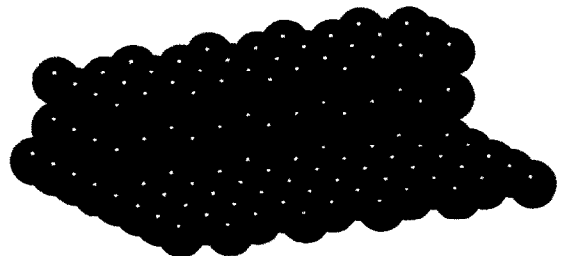


Fig. 6. Doubling of the jagged, $\langle \bar{1}2\bar{1} \rangle$ step on a (111) surface. Note the formation of (311) microfacets.

to facet toward the $[\bar{1}11]$ direction (i.e. another close-packed direction) when doubling occurs; the doubling energy is $-1.3 \text{ meV}/a_1$. The doubling of these steps does not present a barrier to a change in direction of the growth of a Ag{111} surface toward another close-packed plane.

For the jagged step on Ag{111}, the microfacet is (311) oriented at an angle of 60° to the step edge. (Cf. fig. 6.) On this remarkable surface the “excess” step energy associated with doubling is $-99.4 \text{ meV}/\text{exposed (edge) atom}$, i.e. $-114.8 \text{ meV}/a_1$. For the doubling of straight steps on Ag{100}, the microfacet index is {111} and the excess step energy is $-38.1 \text{ meV}/\text{atom}$. The magnitude is much larger than in the case of the {100} step on Ag{111}; doubling clearly lowers of the total energy as the surface facets to {111}. Finally, in the case of the jagged step on Ag{100}, there is microfaceting in the [110] direction. As expected, the excess step energy of doubling is negative, viz. $-2.74 \text{ meV}/\text{apex atom}$, i.e. $-1.94 \text{ meV}/a_1$. The results of these calculations of step doubling energies are summarized in table 2.

3. Defects: adatom and vacancy clusters

In this part of the paper, we begin by carefully analyzing the energetics of adatom and vacancy clusters, then apply the results to kinks and to clusters attached to steps. In all cases, we conserve atoms: the defects come from or go to the bulk, with bulk atom energy -2.85 eV . Because of its high symmetry and negligible corner ener-

gies, the Ag{100} surface is the simpler place to start.

3.1. Vacancy clusters on Ag{100}

To remarkable accuracy the energy, as calculated in EAM, of a single-layer-deep cluster of vacancies is proportional to its perimeter, as measured using $\langle 011 \rangle$ links. The number of these a_1 -long links is always even. Hence, this energy is some integer multiple of 205 meV , twice the step energy per a_1 . More generally, one can form a vacancy cluster from elementary square-plaquette units and assign an energy to each row. The resulting “simple rules” are catalogued in table 3, along with the even simpler “rule” to just find the perimeter (measured along the starting plane, i.e. the top edge of the step at the defect edge), projected onto the principal-axes directions. In only two listed cases are there notable deviations from the perimeter estimate, and these are essentially the same: the energy to remove a single atom from a flat {100} surface is 402 meV , while the perimeter rule predicts 410 meV . Apparently the relaxation around an isolated vacancy is greater than around straight steps in a large structure: extracting one atom from the top layer of a frozen (relaxed) surface costs energy 416 meV . The subsequent growth of a single vacancy into a chain can take place either along a close-packed direction or at 45° . While growth along a close-packed direction costs 206 meV per additional vacancy in the chain, growth at 45° costs about as much as isolated vacancies, 402 meV per

Table 2

The energetic consequences of step doubling on the five previously considered stepped Ag surfaces; generally, steps which facet to form higher (lower) symmetry planes have negative (positive) doubling energy; however, jagged steps which double to (311) and (110) have negative doubling energies

| Type | Initial Miller indices | Separation (a_1 units) | Step direction | Faceting direction | Doubling energy meV/a_1 |
|------------------|------------------------|---------------------------|---------------------|--------------------|----------------------------------|
| (111) straight A | (433) | $10/\sqrt{3}$ | $[01\bar{1}]$ | [100] | + 10.11 |
| (111) straight B | (443) | $11/\sqrt{3}$ | $[\bar{1}10]$ | [111] | - 1.30 |
| (111) jagged | (432) | 3 | $[\bar{1}2\bar{1}]$ | [311] | - 114.8 |
| (100) straight | (711) | $3\frac{1}{2}$ | $[\bar{1}10]$ | [111] | - 38.1 |
| (100) jagged | (810) | $4\sqrt{2}$ | [001] | [110] | - 1.94 |

Table 3
The energies attributed to growth of vacancy clusters on Ag{100} by various types of additions

| sType of addition | Additional energy (meV) | Units of $2\beta a_1$ | (meV) Adatom | equivalent |
|---|-------------------------|-----------------------|--------------|------------|
| Single vacancy | 402 | 2 | → 410 | 458 |
| Single at end of an $\langle 011 \rangle$ chain | 205 | 1 | 205 | 201, 223 |
| Single at 45° | 402 | 2 | 410 | 449 |
| Row larger by two than adjacent row | 614 | 3 | 615 | = |
| Row smaller by two | 203 | 1 | 205 | = |
| Row larger by one | 409 | 2 | 410 | = |
| Row smaller by one | 205 | 1 | 205 | = |
| Row same size | 205 | 1 | 205 | = |
| Row same size, offset one atom | 409 | 2 | 410 | = |

The numbers given are representative and may vary from row to row by about 1 or 2%, indicative of corrections due to slightly longer range effects than those produced by nearest neighbors. Entries “=” in the last column indicate that the value is essentially the same as for vacancies. The energies depend essentially on the number of additional links of length a_1 , each having energy $2\beta a_1$, i.e. $2v$ in units of bond energies, or ~ 204 meV for steps on {100} surfaces (cf. table 1).

vacancy, so that unless vacancies border on a common nearest-neighbor, they do not really belong to the same cluster!

As an illustration of the rules in table 3, we consider an isosceles triangle cluster of 16 vacancies, so with rows of 1, 3, 5, and 7, shown in fig. 7. The full EAM calculation gives an energy of 2.245 eV. The perimeter has 22 links, so the simplest rule predicts an energy of 2.255 eV.

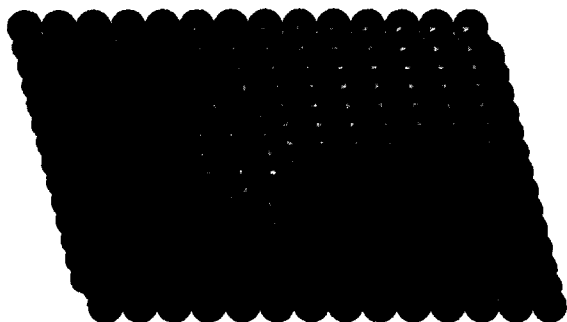


Fig. 7. Vacancy triangle discussed in the text to illustrate the rules in table 3.

From the rules in the table, going from apex down gives 2.244 eV while proceeding up from the base gives 2.241 eV. For another example, we consider a 5×5 square cleaved just to the side of a diagonal, so with rows of 1, 2, 3, 4, and 5 vacancies. The full EAM calculation gives an energy of 2.041 eV, the perimeter rule for 20 links gives 2.050 eV, and the table gives 2.038 eV.

A corollary of the perimeter rule is that vacancy clusters with the same (lattice) perimeter have the same energy, to lowest order, regardless of the number of missing atoms or the shape. We tested this idea on several configurations and found excellent agreement. This corollary could have important implications for mechanisms of cluster diffusion across surfaces. Specifically in this case, clusters of a given number of vacancies prefer square-like arrangements, both globally and locally. If one vacancy begins to diffuse around the periphery, there will be a tendency for others to follow just behind.

3.2. Adatom clusters on Ag{100}

All of the above calculations for vacancies were repeated for adatoms on Ag{100}. The differences are slight enough to require only a brief description. First, the energy of an isolated adatom is 458 meV, thus greater than the vacancy energy. (Cf. table 3.) Thus, single atom excitations violate the up-down or adatom-vacancy symmetry in most models of surfaces used in statistical mechanics, in particular the solid-on-solid model and variants thereof, as discussed in section 3.5. Second, the growth of an adatom chain in a close-packed direction involves the addition of 201 meV for the second atom and 223 meV for each subsequent atom. Third, growth of adatom chains at 45° to close-packed directions costs 449 meV per additional atom, showing an attractive interaction of 9 meV between second-nearest-neighbor pairs on the surface.

Once these differences are accounted for in the creation of an initial chain of adatoms on the surface, the previous rules of table 3 apply for the growth of the cluster, with one exception. Bringing a cluster to an apex by the addition of a single adatom costs the previously calculated 223 meV.

These results have important implications for the calculation of the energy of defects and defect clusters attached to steps, which will be discussed in detail following the description of vacancy and adatom clusters on Ag{111}.

3.3. Vacancy clusters on Ag{111}

A vacancy cluster on Ag{111} has a more complicated symmetry than one on the Ag{100} surface due to the two kinds of straight steps. Since for this element, EAM suggests that the energies of these two straight steps with densely packed edges are nearly the same, we can again, to lowest order, just measure the perimeter (along the crest) in principal directions of the monolayer vacancy cluster and multiply by 189^{-} meV. Again, we can be slightly more accurate by constructing the clusters row by row and by paying attention to whether A or B steps are exposed. The results are summarized in table 4.

As an example, consider equilateral triangles of vacancies, for which all edges have the same type step. Again the elemental process is the formation of a vacancy chain. The energy of a single vacancy on Ag{111} is 549 meV. Each additional hole added to the chain costs 377 meV. Because of the inequality of the different directions of growth on Ag{111}, the counting scheme for calculating the energy of arbitrary clusters on Ag{111} is more complicated than for Ag{100}. Nevertheless, the results of the tabu-

lated calculations represent a complete set of operations by which the EAM energy of any arbitrary cluster can be closely estimated: one simply finds an apex of the cluster and assigns it the energy of a single vacancy, then moves across the cluster, calculating and adding the energy of each row by the rules presented in the table.

3.4. Adatoms on Ag{111}

As in the case of Ag{100}, similar calculations were done with adatom clusters on Ag{111}. The results are similar; except for the formation of an initial triangle or two rows of adatoms, the growth of these clusters proceeds along the same energetic basis as the growth of vacancy clusters. They are almost entirely symmetric.

Like for vacancies, the energy of an adatom triangle on the surface is independent of the orientation. In our EAM calculations the two possible orientations are the same, both +1.221 eV. A count of the total coordination of the 3 adatoms and their 7 nearest neighbors in the original surface shows that the total coordination of the 10 atoms is 87 in either case [38]. From this perspective, the coordination number is the key to understanding EAM energies of localized defect systems of close-packed systems.

The formation of an adatom chain on Ag{111} costs 709 meV for the first adatom, 379 meV for the second, and 417 meV for each additional adatom. As stated before, the subsequent addi-

Table 4

The cost in surface energy of increasing the size of a vacancy cluster on clean Ag{111} in a variety of different ways

| Type of addition to cluster | Energy cost (meV) | $2\beta a_1$ -units | (meV) | Adatom equivalent |
|-----------------------------|-------------------|---------------------|--------------|-------------------|
| Single vacancy | 549 | 3 | 566 | 709 |
| Vacancy to a chain | 377 | 2 | 377 | 379, 417 |
| Row larger by one | 562/568 | 3 | 566 | = |
| Row the same size | 385 | 2 | 377 | = |
| Row smaller by one | 185/192 | 1 | 189 | = |
| Row larger by $1 + n$ | $582/578 + 377n$ | $3 + 2n$ | $566 + 377n$ | = |
| Row smaller by any integer | 197/202 | 1 | 189 | = |

While the list does not exhaust the incremental changes which can be made, any vacancy cluster can be built up by a series of operations equivalent to the changes listed in this table. When two numbers are listed, with a "/" between them, the first refers to an A or [100]-microfacet step, while the second refers to a B or [111]-microfacet step. Again, each unit of βa_1 (each increase of the perimeter by one) corresponds to two lost nearest-neighbor bonds and an energy of ~ 189 meV (cf. table 1).

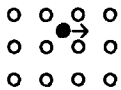
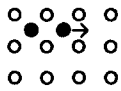
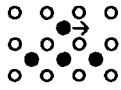
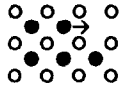
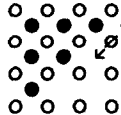
tion of rows to an adatom cluster is very similar to the operations on a vacancy cluster, with all of the energies in table 5 incremented by corrections of around 50 meV. One exception is in the addition of the first row in the formation of a triangle by adding smaller rows. Once the initial vacancy chain is established, it costs virtually nothing to add the second, smaller row. Subsequently, the cluster grows in the same way as a vacancy cluster. Interestingly, the energy recovered by the system because of the null cost of adding the second row is enough to make the total energy of large clusters nearly symmetric between vacancies and adatoms. For example, the energy of a system of two rows that are 4 and 3 vacancies (adatoms) wide is +1.871 (+1.920) eV.

3.5. Symmetries and lattice models

The adatom–vacancy symmetry that is implicit in most models of stepped surfaces, e.g. TSK and SOS, is generally well obeyed by the calculated energies. Isolated defects are the glaring exception: adatom excitation requires 12% more energy than vacancy excitation for Ag{100} and 29% more on Ag{111}. As indicated in tables 3 and 4, the adatom energies are much higher than predicted from the perimetric bond-counting scheme, while the vacancy energies are a few percent lower. The asymmetry points up the crucial role that coordination number plays in EAM (presumably reflecting the actual behavior in these metals) and underlines the many-body character of the EAM potentials. Without relaxation, the asymmetry would be even greater: on Ag{111} the defect energy increases nearly half way to the bond-count value, while the adatom energy increases by roughly 100 meV. The adatom relaxes by drawing 0.2 Å closer to the substrate, increasing the charge density at its center and so its embedding energy. For large defects, relatively small asymmetries appear in the corner energies. Overall, this discussion should be taken as more qualitative than most presented above, given the exceptional non-uniformity of the charge distribution around an adatom.

Table 5

A comparison of calculated barriers to diffusion (in meV) in Voter's dynamic simulations [13], using Voter–Chen embedding functions, and in our simpler static models, using FBD-U3 functions

| Hop | Adatom | | Vacancy | |
|--|-------------------|--------|------------|--------|
| | Voter [13] | Static | Voter [13] | Static |
| (a)  | 491 ^{a)} | 479 | 465 | 473 |
| (b)  | 774 | 721 | 509 | 494 |
| (c)  | 257 | 257 | 478 | 517 |
| (d)  | 504 | 543 | 513 | 543 |
| (e)  | | 457 | | 457 |

In the sketch, open circles indicate topmost complete layer of atoms; the filled circles indicate adatoms for the left columns and vacancies in an otherwise complete layer for the right columns. Agreement between Voter's and our numbers should be best in (c), where we can freeze the adatom in the direction parallel to the step edge and allow it to relax into the saddle point of the potential in both other directions. In (d) and (e), only one calculation was done for each structure, because of the symmetry between vacancy and adatom systems with these configurations.

^{a)} The activation energy was later computed to be 480 meV with AFW or VC potentials [7]. Analogous calculations [46], both the classical barrier and with dynamic simulations, using DePristo's corrected effective medium theory gave this energy as about 240 meV, with the remark that Ag adatoms have anomalously low barriers compared to other late transition and noble species.

For Ag{111} the Boltzmann weights at room temperature associated with isolated adatoms and vacancies are 5×10^{-13} and 3×10^{-10} , respec-

tively. These small probabilities suggest that any isolated defects found on Ag at room temperature are unlikely to come from equilibrium fluctuations. While adatoms have not generally been seen in STM experiments [16], the rapid step fluctuations do suggest highly mobile adatoms, as discussed below. Around 1200 K, the respective weights become 8×10^{-4} and 4×10^{-3} , which would be observable with STM. (This discussion neglects the contribution of entropy, both configurational and vibrational [39], which will considerably influence the probability of observing these defects.) The prediction then would be that nearly an order of magnitude more vacancies than adatoms should be found.

The implication of this asymmetry for statistical mechanics is that in detailed attempts to model metal surfaces, simple spin Hamiltonians must be augmented by three-site terms to account for the adatom-defect asymmetry. Such terms can have important effects at preroughening (but not roughening) transitions [40]. More generally, their neglect will distort estimates of pair energies [41].

A more serious caution is that the nearest-neighbor bond picture is not an adequate approximation for all systems for which EAM is a viable technique. Specifically, Wright et al. [42] calculated energetics of clusters of Pt, Pd, and Ni on Pt(001). For all three adspecies, viewed as two-dimensional lattice gases with a *frozen* substrate, the nearest-neighbor interaction is attractive, the second-neighbor interaction is repulsive, and the leading trio interaction is attractive. However, for Ni the nearest-neighbor attraction is unusually small (and the others relatively large), with the consequence that the energetics favor clusters of Ni adatoms forming chains rather than compact islands. When the substrate is allowed to relax, they find that Pd trimers and Pt trimers and pentamers also prefer linear configurations, although other sizes still are compact. While such behavior has been observed for Pt using FIM [9], the more drastic behavior of Ni/Pt(001) has not, perhaps because the Ni exchanges with substrate Pt [42,43]. Apparently when the relaxation is strong enough to produce chains, it also leads to diffusion by an exchange mechanism [42].

On the close-packed Pt{111} surface, compact clusters, at least those of Pt, are stable for all sizes [44]. (Studies of these clusters described their energies in terms of lateral interactions that depended on distance from the edge [44]. These effects could presumably also be explained in terms of multi-site interactions [41].) In summary, unconventional behavior is most likely to occur in bimetallic systems with smaller adatoms on an open substrate plane with larger atoms. Then the direct interaction between neighboring adatoms may be anomalously weak, causing much of the interaction to be indirect and so much smaller and rather unpredictable in sign [45].

3.6. Vacancy and adatom clusters at steps

Using these results for local defect systems, we can assess the energies of pairs of kinks such as might be excited thermally in regular step structures. The energies we have calculated for these defects are in the thermal range, and the preceding calculations on flat Ag can be applied without modification to stepped structures. From the point of view of an atom on the terrace of a regularly stepped surface, the step and adjoining terrace in the uphill direction is a large adatom cluster which goes off to infinity in two directions. The terrace in the downhill direction is similarly a large vacancy cluster. We argue that adding vacancies or adatoms to these two extensive clusters is precisely the same, within the limitations of EAM, as the calculations we have already done. Again, from the simplest viewpoint, the attachment of a cluster to a step is a reduction in perimeter by *twice* the length of contact, since both cluster and step decrease their boundary. (Of course, the actual binding energy should increase if the step edge after dislodging a cluster has many kinks and decrease if the cluster takes on a more compact configuration than it had when attached.) Two sample calculations on Ag{111} adequately corroborate the viability of estimation based on the perimeter.

First we introduced a chain of vacancies along a step edge. We repeated this calculation for several chain lengths and on both kinds of close-packed steps on Ag{111}. The results show that

Table 6
The potential barriers (in meV) to diffusion of adatoms and vacancies on clean stepped Ag{111}

| Hop | Adatoms | Vacancies |
|-----|------------------|-----------|
| (a) | 60 ^{a)} | 314 |
| (b) | 121 | 314 |
| (c) | 275 | n/a |
| (d) | 207 | n/a |
| (e) | 379 | 379 |
| (f) | 326 | 326 |
| (g) | n/a | 408 |
| (h) | n/a | 384 |

the energy of the kink/anti-kink pair formed by the chain is independent of the length of the chain, even for the removal of a single atom, and that the total energy of the defect system is equal to the energy given in table 4 for the energy of adding a row to a vacancy cluster that is smaller than the previous row by 2 or more atoms, 202 or 197 meV for a surface with a $\langle 100 \rangle$ or close-packed step, respectively. From this point the energy of any wandering step that eventually comes back to its low temperature equilibrium location can be calculated by simply applying the operations in table 6. To check this assertion, a randomly selected excitation of 28 vacancies with irregular geometry was introduced onto a $\langle 100 \rangle$ step. The estimated EAM energy of the defect system was +1.542 eV. The result of the actual EAM run was +1.572 eV, giving an error for the estimate of 2%.

In the second test, we created a pair of defect systems in which one had an adatom cluster growing onto the downhill terrace and the other had a vacancy cluster growing onto the uphill terrace with the same shape. The discussion above would indicate that the energy should be nearly the same. The adatom cluster was chosen to be of the same shape as the 28 atom vacancy cluster previously calculated. The result was that the energy of the adatom cluster attached to the step was +1.583 eV, which is within 1% of the calculated value of the vacancy cluster energy.

Notes to table 6:

The notation for open and filled circles is the same as in table 5. The behavior for adatoms in the first several cases is strikingly different from {100}, listed in table 5. Configuration (a) shows a very weak corrugation for single adatoms on clean {111}. For other geometries the numbers are roughly similar to those on {100}.

^{a)} Liu et al. [7] computed the activation energy to be 59 or 44 meV with AFW or VC potentials, respectively. Rilling et al. [6] found 58 meV.

4. Barriers to diffusion

In addition to estimating the energy of vacancy or adatom clusters on vicinal surfaces, EAM can also be used to investigate barriers to their diffusion across a surface. This section is patterned after Voter's EAM-based molecular dynamics simulations [13] in which large ($n > 50$) vacancy and adatom clusters were allowed to diffuse across Ag{100}. He catalogued all the hopping transitions between configurations and carefully calculated the barriers involved. We use Voter's work as a benchmark for the accuracy of our simple static approach and extend the work to similar calculations for Ag{111}, where only adatom diffusion on flat surfaces has been previously considered [7]. We also compare with other studies of diffusion on flat Ag surfaces [6,46].

Here, we straightforwardly constructed the surface prior to the transition and calculated the energy, then moved the adatom or vacancy in question to the geometric saddle point between the positions before and after the diffusive hop and recalculated the energy [47]. The difference is reported as the barrier to diffusion. In cases where the geometric saddle point is not obviously the saddle point of the interatomic potential, we fixed the adatom in one direction and allowed DYNAMO to find the actual saddle point of the potential by minimizing the energy. Our numbers agreed best with Voter's when we could follow this procedure. In assessing agreement, we recall that Voter parameterized his EAM functions for these calculations. The results of our calculations for several geometries are given in table 5, along with Voter's numbers.

Some qualitative trends are evident from this table. We see that the diffusion barrier for adatom motion next to a straight step edge is much lower than that across a terrace, while for vacancies there is little change. In contrast, there is only a minor advantage to diffusing along a jagged step, suggesting that transport will be enhanced along straight steps and that dynamic processes will pile adatoms at the end of straight segments, promoting kinetically the growth of these "facets".

The results of similar calculations of diffusion barriers [48] on Ag{111} are given in table 6.

There are some remarkable differences between the results for {111} surfaces and for {100} surfaces. As also noted by others [6,7], on {111} the barrier for an isolated adatom to hop to an adjacent threefold symmetry site is very small, about 12% of the {100} barrier. Thus, single adatoms can wander rather freely on the clean surface until it comes in contact with a step, another adatom, or a defect. On the other hand, the barrier to diffusion along either kind of straight step is several (roughly 4) times as large. Over some intermediate temperature range, then, adatoms can travel readily across flat regions but become essentially immobile after contacting other adatoms. This condition leads to diffusion-limited aggregation (DLA) [49], i.e. the growth of dendritic islands with fractal boundaries rather than compact clusters. Such islands in fact have been observed with STM for Au atoms on Ru(0001) [50] at room temperature and for Pt islands on Pt{111} [51] at 205 K, as well as many other examples of late-transition-metal atoms on the close-packed face (but with counterexamples such as Co adsorption) [52]. At higher temperatures, the edges of the islands become smoother and their structure more compact. For vacancies, the barrier for motion across terraces is much higher, and closer to that for vacancy motion near step edges. Hence, in an evaporation experiment, any tendency to form non-compact islands would be far weaker.

Another trend consistent with experiment is the lower barrier for diffusion along A steps (row (d) of table 6) than B steps (row (c)) at low temperature. Such behavior was clearly seen by Wang and Ehrlich [53] in FIM measurements of diffusion of Ir atoms around Ir₁₂ islands on Ir{111}; they found this behavior consistent with expectations because along A steps the peripheral atom stays closer to the other atoms as it moves. From STM measurements of island shapes of Pt on Pt{111} Michely et al. [54] deduced greater diffusion along A steps. In earlier FIM experiments it was likewise found that the activation energy for diffusion on (331) surfaces (presumably along B steps) is larger than on (311) surfaces (a limiting case of A steps) of Ni, Rh, and Pt [55]. It is noteworthy that at higher tem-

peratures, diffusion along B steps eventually exceeds that along A steps, with remarkable consequences [54].

On both {100} and {111} we see that the barrier for an adatom near an edge nearly doubles when the adatom starts with a neighbor at one side. This common result suggests that it is substantially more difficult for an adatom to “separate from a kink” (i.e. for the kink to retreat one spacing) than for an adatom to move along the edge. Pairs of adatoms tend to provide growth centers, since there is an added energy for them to separate into monomers; in contrast, the barrier for the separation of pairs of vacancies is comparable to the barrier for monomer diffusion.

It is not clear how to interpret the remarkable frizzled nature of steps observed on Ag{111} [16]. While this behavior is characterized by high kink mobility, rapid adatom motion along the edges would seem inconsistent with the results just described for DLA-like islands. Perhaps the behavior results from rapid attachment and detachment of adatoms to the step edges. The dynamics associated with the two kinds of mechanisms should be readily distinguishable [56] at lower temperatures.

We recall from tables 3 and 4 that the difference between the {111} and {100} surfaces is also rather large, with adatoms on the {100} surface bound somewhat more strongly to their positions than vacancies. Of course, an adatom or vacancy on {100} has the same number of nearest neighbors, while a vacancy on {111} has twice as many nearest neighbors as an adatom. The wide disparity between the barrier heights disappears after the clusters on {111} build to a reasonable size. Vacancies have barrier heights for single defects of the same order of magnitude as larger vacancy systems, such as the step terrace systems in (c) through (h) of table 6.

Our tables do not consider alternate modes of diffusion. Liu et al. [7] demonstrated that concerted substitution of adatoms [57] (exchange with substrate atoms) is the dominant diffusion mode on flat {100} surfaces of Pd, Pt, and Au (but not Ni, Cu [58], or Ag). Tian and Rahman [8] also found evidence that on vicinal Cu{100} the down-step diffusion of adatoms is aided by a concerted

event in which the adatom replaces a step edge atom and the edge atom moves onto the terrace as an adatom.

5. Spring constants for adatom vibrations

Finally we investigate the vibrations of adatoms on vicinal surfaces, particularly those with straight steps, in a quasi-static approach. The purpose of these calculations is to assess how much these vibration frequencies change as adatoms approach a step from an open terrace. Specifically, we moved adatoms toward and away from the surfaces incrementally, froze them in the displaced positions and calculated the change in the potential energy while letting the substrate relax. We only investigated vibrations perpendicular to the terrace, both for calculational reasons and because of the experimental ability to measure such vibrations using IR spectroscopy.

We fit the energies from points along the trajectory, at 0.1 \AA intervals up to 1 \AA away from the equilibrium height, to polynomials initially up to 4th order. We then removed the anharmonicity by truncating the data sets until a simple quadratic polynomial sufficed in the fit, as measured by a scatter plot of the difference between the numbers and the fitted curves. By restricting the height range to $\pm 0.6 \text{ \AA}$ from equilibrium, still quite sizable, we obtained good quadratic fits, with no discernable anharmonic character.

The results of the calculations are reported in table 7 as the spring constant K for a particular vibration, in $\text{eV}/\text{\AA}^2$ [59]. We see that on a {111} terrace, K decreases by nearly 10% when the adatom is adjacent to either of the close-packed steps. In contrast, on a {100} terrace, where K is 20% lower than on a {111}, it increases by 5% near a straight step. Such trends should be observable experimentally.

In a brief attempt to assess transverse modes, we searched for energetically favored directions for the motion by calculating the energy of the system for displacements of 0.5 \AA at all multiples of 5° from the vertical for the case of an adatom adjacent to an A step on a {111}. The energy decreased monotonically as the displacement di-

Table 7
Computed effective harmonic spring constants for adatoms vibrating normal to the low-index Ag facets

| Adatom position | K (eV/Å ²) |
|----------------------------------|--------------------------|
| On flat {111} | 2.39 |
| Adjacent to A (<110>/{100}) step | 2.22 |
| Adjacent to B (<110>/{111}) step | 2.21 |
| On flat {100} | 1.98 |
| Adjacent to straight step | 2.10 |

Polynomials were fit to energies evaluated at 0.1 Å intervals from the equilibrium height. By restricting the height range to ± 0.6 Å from equilibrium, still quite sizable, we could obtain good fits to quadratics, with no discernable anharmonic character.

Typically, $X_r^2 = 1.3$ for fitted curves, and all the computed energies in our truncated ($|\Delta z| \leq 0.6$ Å) sets lie within one standard deviation of the fitted curve.

Evidently the perpendicular oscillation frequency changes by no more than 10% when the atom is near a step edge.

rection approached horizontal. From a chemical viewpoint, we implicitly assume that since the bonds between the adatom and the step are perpendicular to the motion, they are stretched only slightly and so contribute little to the energy compared to the vertically stretched bonds between the adatom and its three nearest neighbors on the terrace. Then we may also suppose that the 5–10% difference between the spring constants associated with the adatom being near and far from a step gives a measure of the effect of these perpendicular bonds to the vertical modes.

For comparison, we mention more thorough EAM studies by Tian and Black [60] of phonon spectra and mean-square displacements of the substrate atoms of straight-stepped surfaces vicinal to Cu{100}. They find that normal vibration frequencies for atoms of the step edge are *lower* than those of terrace atoms. Correspondingly, the perpendicular (to the terrace plane) room-temperature mean-square displacements increase by up to 5% and slightly less for the penultimate terrace atom. The transverse displacement for the edge atom increases far more.

6. Conclusions

We have illustrated how EAM can be used to estimate properties of interest for vicinal Ag{100}

and {111}, especially step and kink energies. As anticipated by simple statistical mechanical models, we can rather accurately account for these tabulated properties using a nearest-neighbor bond approximation with bond energy $\sim 10^2$ meV (a much smaller value than obtained by fitting the (bulk) cohesive energy in the same approximation). Also in accord with these models, adatom–vacancy symmetry is a good approximation, *except*, however, for single defects. Simple bond counting again leads to good estimates of cluster energies and their binding to step edges. Some of our results can be compared with experiments. The ratio of the two kinds of straight steps on Pt{111} in EAM is much closer to unity than measured, but at least, in contrast to Ag, B steps are favored. It would be interesting to find experimentally whether A steps are actually preferred on Ag. (Furthermore, it would be worthwhile to test the conjecture that A steps are (more strongly) favored on Ni and Cu. The situation on Au{111} (B steps favored?) is clouded by its reconstruction [61].) Another open question is what the step and kink energies are on Ag{110}, a system of recent interest [62]. Presumably a calculation including gradient corrections [11,14] could remove the spurious reconstruction [10] to allow consideration of the needed configurations.

Our results have implications for surface morphology: step doubling is favored in many cases and can be described in terms of microfacet formation. As might be expected, we find that diffusion on {111} is quite different from that on {100}, and proximity to steps alters barriers significantly, increasing them, surprisingly, on {111}. Other general features are also consistent with experiment. The thermal dependence of these properties will require more sophisticated investigation, presumably using molecular dynamics. Finally, steps are found to modify modestly (but of measurable size) the spring constant for vibrations normal to terraces, increasing it on {100}, decreasing it on {111}.

Acknowledgements

This work was supported in part by NSF-MRG grant DMR 91-03031. R.C.N. acknowledges sup-

Table 8
Displacements of atoms on an 8-atom wide Ag{111} terrace bounded by B steps

| Terrace row | Δz_{12} (Å) | $\Delta x_{n,n+1}$ (Å) |
|-------------|---------------------|------------------------|
| Top edge | -0.0660 | -0.0380 |
| Row 1 | -0.0347 | -0.0068 |
| Row 2 | -0.0344 | -0.0055 |
| Row 3 | -0.0338 | -0.0040 |
| Row 4 | -0.0336 | -0.0031 |
| Row 5 | -0.0359 | -0.0012 |
| Row 6 | -0.0340 | -0.0012 |
| Bottom edge | -0.0066 | |

The displacements in the x -direction compress the terrace and stretch the step tread. The displacements of the top and bottom atoms at the step also stretch the step, when compared to the displacements of the flat surface.

port from the United States Army. We thank N.C. Bartelt, R.L. Blumberg Selinger, Th. Michely, E.D. Williams, and D.R. Eisner for useful discussions, N.C.B. and R.L.B.S. for helpful comments on the manuscript, and D.R.E. for help in producing the figures. We are especially grateful to M.S. Daw and S.M. Foiles for use of the code DYNAMO 7.6 and several fruitful conversations, and to A.F. Voter for providing us with his EAM functions in a convenient format. We thank J.E. Black, Z.-J. Tian, R. Lynden-Bell, and Th. Michely for supplying unpublished information.

Appendix. Atomic relaxations near a step

In this appendix we illustrate the atomic relaxations of first-layer atoms near a step. As a representative example, we choose the B step on the Ag{111} surface. The numbers given in table 8 are relaxations from unreconstructed bulk lattice spacings and may be compared to the first-layer relaxation of the flat {111} surface of $\Delta z_{12} = -0.0319$ Å and the row spacing of the {111} surface of $x_{nm} = 2.4842$ Å.

References

- [1] M.S. Daw and M.I. Baskes, Phys. Rev. B 29 (1984) 12; For a recent review, see: M.S. Daw, S.M. Foiles and M.I. Baskes, Mater. Sci. Rep. 9 (1993) 251.
- [2] J.S. Nelson, M.S. Daw and E.C. Sowa, Phys. Rev. B 40 (1989) 1465.
- [3] N. Luo, W. Xu and S. Shen, Phys. Status Solidi (b) 158 (1990) 493.
- [4] L. Yang, T.S. Rahman and M.S. Daw, Phys. Rev. B 44 (1991) 13725.
- [5] J.B. Adams, S.M. Foiles and W.G. Wolfer, J. Mater. Res. 4 (1989) 102.
- [6] W.K. Rilling, C.M. Gilmore, T.D. Andreadis and J.A. Sprague, Can. J. Phys. 68 (1990) 1035.
- [7] C.L. Liu, J.M. Cohen, J.B. Adams and A.F. Voter, Surf. Sci. 253 (1991) 334; G.L. Kellogg and A.F. Voter, Phys. Rev. Lett. 67 (1991) 622.
- [8] Z.-J. Tian and T.S. Rahman, Phys. Rev. B 47 (1993) 9751.
- [9] P.R. Schwoebel, S.M. Foiles and C.L. Bisson, Phys. Rev. B 40 (1989) 10639.
- [10] S.M. Foiles, Surf. Sci. 191 (1987) L779.
- [11] L.D. Roelofs, S.M. Foiles, M.S. Daw and M.I. Baskes, Surf. Sci. 234 (1990) 63.
- [12] S.M. Foiles, M.I. Baskes and M.S. Daw, Phys. Rev. B 33 (1986) 12.
- [13] A.F. Voter, in: Modeling of Optical Thin Films, Ed. M.R. Jacobson, SPIE 821 (1987) 214.
- [14] M.S. Daw, Phys. Rev. B 39 (1989) 7441.
- [15] D. Wolf, Surf. Sci. 226 (1990) 389.
- [16] M. Poensgen, J.F. Wolf, J. Frohn, M. Giesen and H. Ibach, Surf. Sci. 274 (1992) 430.
- [17] J.K. Nørskov, K.W. Jacobsen, P. Stoltze and L.B. Hansen, Surf. Sci. 283 (1993) 277.
- [18] C. Jayaprakash, C. Rottman and W.F. Saam, Phys. Rev. B 30 (1984) 6549.
- [19] E.D. Williams and N.C. Bartelt, Science 251 (1991) 393, and references therein.
- [20] J.F. Nicholas, An Atlas of Models of Crystal Surfaces (Gordon and Breach, New York, 1965).
- [21] M. Wortis, in: Chemistry and Physics of Solid Surfaces VII, Eds. R. Vanselow and R. Howe (Springer, Berlin, 1988) p. 367 (esp. p. 395).
- [22] A.F. Voter and S.P. Chen, Mater. Res. Soc. Symp. Proc. 82 (1987) 375.
- [23] B.D. Todd and R.M. Lynden-Bell, Surf. Sci. 281 (1993) 191.
- [24] A.P. Sutton and J. Chen, Philos. Mag. Lett. 61 (1990) 139.
- [25] Th. Michely and G. Comsa, Surf. Sci. 256 (1991) 217.
- [26] (a) S.C. Wang and G. Ehrlich, Phys. Rev. Lett. 67 (1991) 217; (b) Th. Michely, private communication.
- [27] M.A. Van Hove and G. Somorjai, Surf. Sci. 92 (1980) 489.
- [28] D.R. Eisner and T.L. Einstein, Surf. Sci. Lett. 286 (1993) L559. In fig. 1 of this letter, the subscripts of b_1 and b_2 are reversed. In the equation for w_p preceding eq. 7, all signs should be +. In the final form of eq. (9), " $n_2 - 1$ " should be " $n_1 - 1$ ".
- [29] K.D. Hammonds and R.M. Lynden-Bell, private communication, 1993, found $\beta = 700$ K/Å for Ag(211).

- [30] C. Herring, *Phys. Rev.* 82 (1951) 87.
- [31] B. Schwartzentruber, Y.-W. Mo, R. Kariotis, M.G. Lagally and M.B. Webb, *Phys. Rev. Lett.* 65 (1990) 1913.
- [32] N.C. Bartelt, T.L. Einstein and E.D. Williams, *Surf. Sci.* 276 (1992) 308.
- [33] Specifically, this condition requires that mirror planes pass through sites along the step edge, perpendicularly to the mean direction of the step edge.
- [34] K.D. Hammonds and R.M. Lynden-Bell, *Surf. Sci.* 278 (1992) 437.
- [35] R.C. Nelson, Master's thesis, University of Maryland, 1992, unpublished.
- [36] D. Wolf and J.A. Jaszczak, *Surf. Sci.* 277 (1992) 301.
- [37] T.L. Einstein, T.M. Jung, N.C. Bartelt, E.D. Williams and C. Rottman, *J. Vac. Sci. Technol. A* 10 (1992) 2600.
- [38] One orientation requires all 7 surface atoms to count all of the nearest-neighbor bonds of the adatoms; the other requires only 6, while the 7th, with a flat surface coordination of 9, is added for symmetry.
- [39] See, e.g., F. Agullo-Lopez, C.R.A. Catlow and P.D. Townsend, *Point Defects in Materials* (Academic Press, London, 1988) chs. 2, 11.
- [40] M. den Nijs, *Phys. Rev. Lett.* 64 (1990) 435.
- [41] T.L. Einstein, *Langmuir* 7 (1991) 2520.
- [42] A.F. Wright, M.S. Daw and C.Y. Fong, *Phys. Rev. B* 42 (1990) 9409;
G.L. Kellogg, A.F. Wright and M.S. Daw, *J. Vac. Sci. Technol. A* 9 (1991) 1757.
- [43] G.L. Kellogg and P.J. Feibelman, *Phys. Rev. Lett.* 64 (1990) 3143.
- [44] M. Fallis, M. Daw and C.Y. Fong, *Bull. Am. Phys. Soc.* 38 (1993) 219.
- [45] T.L. Einstein, in: *Chemistry and Physics of Solid Surfaces*, Vol. 2, Ed. R. Vanselow (CRC Press, Boca Raton, FL, 1979) T.L. Einstein, in: *Handbook of Surface Science: Physical Structure*, Ed. W.N. Unertl (Elsevier, Amsterdam, in press).
- [46] D.E. Sanders and A.E. DePristo, *Surf. Sci.* 260 (1992) 116.
- [47] L.D. Roelofs, J.I. Martin and R. Sheth, *Surf. Sci.* 250 (1991) 17.
- [48] For the calculations on {111}, the point at which the potential barrier was measured was the geometric saddle point between adjacent adsorption/desorption sites. If we pin a diffusing adatom/vacancy in its position along the direction of diffusion, it would invariably relax along a perpendicular direction to its original position; hence, the only relaxations we could allow are in the direction perpendicular to the surface.
- [49] H.E. Stanley and N. Ostrowsky, Eds., *On Growth and Form: Fractal and Non-Fractal Patterns in Physics* (Nijhoff, Boston, MA, 1986).
- [50] R.Q. Hwang, J. Schröder, C. Günther and R.J. Behm, *Phys. Rev. Lett.* 67 (1991) 3279.
- [51] M. Bott, Th. Michely and G. Comsa, *Surf. Sci.* 272 (1992) 161.
- [52] R.J. Behm, private communication, 1992.
- [53] S.C. Wang and G. Ehrlich, *Surf. Sci.* 239 (1990) 301.
- [54] Th. Michely, M. Hohage, M. Bott and G. Comsa, preprint.
- [55] D.W. Bassett and P.R. Webber, *Surf. Sci.* 70 (1978) 520; R.T. Tung and W.R. Graham, *Surf. Sci.* 97 (1980) 73.
- [56] N.C. Bartelt, J.L. Goldberg, T.L. Einstein and E.D. Williams, *Surf. Sci.* 273 (1992) 252.
- [57] P.J. Feibelman, *Adv. Mater.* 4 (1992) 394.
- [58] L. Hansen, P. Stoltze, K.W. Jacobsen and J.K. Nørskov, *Phys. Rev. B* 44 (1991) 6523, using effective-medium theory, do find the exchange mechanism to be important for Cu on Cu(100).
- [59] Typically, $X_r^2 = 1.3$ for fitted quadratic curves with calculated points every 0.1 Å and the correlation coefficients are within 1.0 ± 0.1 . All the computed energies in our truncated sets lie within one standard deviation of the fitted curve.
- [60] Z.-J. Tian and J.E. Black, *Bull. Am. Phys. Soc.* 38 (1993) 66, private communication; to be published.
- [61] M.A. Van Hove, R.J. Koestner, P.C. Stair, J.P. Biberian, L.L. Kesmodel, I. Bartos and G.A. Somorjai, *Surf. Sci.* 105 (1981) 189;
R. Ravelo and M. El-Batanouny, *Phys. Rev. B* 40 (1989) 9574, and references therein.
- [62] J.S. Ozcomert, W.W. Pai, N.C. Bartelt and J.E. Reutt-Robey, *Surf. Sci.* 293 (1993) 183;
W.W. Pai, J.S. Ozcomert, N.C. Bartelt and J.E. Reutt-Robey, *Bull. Am. Phys. Soc.* 38 (1993) 342.